

Polarization ellipticity compensation in polarization second-harmonic generation microscopy without specimen rotation

Chen-Kuan Chou*

Wei-Liang Chen*

Peter Tramyon Fwu

National Taiwan University
Department of Physics
No 1 Sec 4 Roosevelt Road
Taipei 106, Taiwan

Sung-Jan Lin

National Taiwan University
Institute of Biomedical Engineering
No 1 Sec 4 Roosevelt Road
Taipei 106, Taiwan

Hsuan-Shu Lee

National Taiwan University Hospital
Department of Internal Medicine
No 7 Chung San South Road
Taipei 106, Taiwan

Chen-Yuan Dong

National Taiwan University
Department of Physics
No 1 Sec 4 Roosevelt Road
Taipei 106, Taiwan
E-mail: cydong@phys.ntu.edu.tw

Abstract. In imaging anisotropic samples with optical microscopy, a controlled, polarized light source can be used to gain molecular information of fibrous materials such as muscles and collagen fibers. However, the delivery of the polarized excitation light source in a system such as a laser scanning optical microscope often encounters the problem of the polarization ellipticity altering effects of the optical components. Using a half-wave plate and a quarter-wave plate, we demonstrate that the polarization ellipticity altering effect of the dichroic mirror in an epi-illuminated multiphoton laser scanning microscope can be corrected, and that this approach can be used to obtain polarized second-harmonic generation (SHG) images of rat tail tendon and mouse leg muscle. The excitation polarization dependence of the SHG intensity is fitted to determine the ratio of the second-order susceptibility tensor elements associated with type I collagen in the rat tail tendon and myofibril in the mouse leg muscle. Our methodology can be applied to polarized SHG imaging without sample rotation. This approach has great potential for imaging noncentrosymmetric biological samples, providing structural information on the molecular scale in addition to morphological information of tissues. © 2008 Society of Photo-Optical Instrumentation Engineers. [DOI: 10.1117/1.2824379]

Keywords: polarization-sensitive devices; multiphoton microscopy; second-harmonic generation.

Paper 07228RR received Jun. 22, 2007; revised manuscript received Oct. 9, 2007; accepted for publication Oct. 9, 2007; published online Jan. 2, 2008. This paper is a revision of a paper presented at the SPIE conference on Multiphoton Microscopy in Biomedical Sciences VII, Jan. 2007, San Jose, California. The paper presented there appears (unrefereed) in SPIE Proc. 6442.

1 Introduction

Optical imaging techniques such as confocal laser scanning and multiphoton imaging have revolutionized biological optical microscopy.^{1,2} In specific applications, polarization microscopy can provide optical structure information that is absent from intensity imaging alone.³⁻⁵ Recently, second-harmonic generation (SHG) microscopy has become an important imaging modality in biological sciences.^{6,7} Biological structures such as muscles, tendons, and corneas are strong generators of second-harmonic signals.^{8,9} With a pulsed femtosecond laser as the excitation source, SHG microscopy has been demonstrated to be an effective, minimally invasive imaging tool for biomedical studies in a wide array of areas including the interaction of cell with extracellular matrix, cancer growth, keratoconus, and skin thermal damage.¹⁰⁻¹³ In addition to morphological information, the polarization dependence of the SHG signal can provide structural information below the resolution of optical microscopy.⁸ Although SHG produces strong forward scattering signals, *in vivo* studies

with optical microscopes usually require epi-illuminated detection. In this configuration, a dichroic mirror is required to separate the excitation source and the emission signal.² Since the reflective properties of dichroic mirrors can alter the polarization ellipticity of the incident excitation light, polarization studies in an SHG laser scanning microscope are often performed by fixing the excitation polarization while rotating the samples.^{8,14} However, the sample rotation approach requires the precise alignment of the observation area to the center of the sample rotation stage, and this causes increased difficulties for *in vivo* microscopic observation, which often requires specialized animal-mounting devices.^{15,16} In addition, subsequent analysis of polarization-resolved images is complicated by processing specimen images at different angular orientations. Therefore, we propose a generalized method using wave plates to compensate for the ellipticity altering effects of optical components such as that caused by a dichroic mirror. Mathematical analysis was performed to demonstrate the application of this approach in delivering linearly polarized excitation light of the desired direction onto the sample. We also obtained the polarization dependence of the SHG signal of a rat tail tendon and a mouse leg muscle. The

*These authors contributed equally to this work.

Address all correspondence to Chen-Yuan Dong, Department of Physics, National Taiwan Univ., Department of Physics - National Taiwan University, Taipei, Taiwan 106 Taiwan; E-mail: cydong@phys.ntu.edu.tw

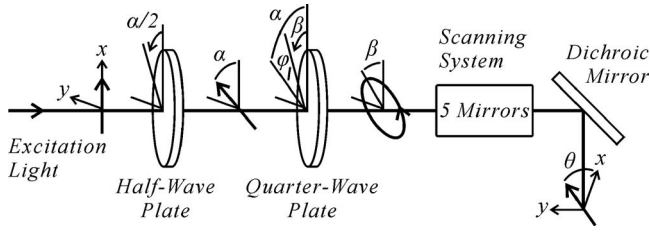


Fig. 1 Ellipticity compensation using half- and quarter-wave plates.

second-order susceptibility tensor element ratios derived from our data are compared with previously obtained results. It was shown that nonlinear susceptibility can be used to infer molecular structures of biological samples.^{14,17,18} Our work has potential application in monitoring structural changes of biological samples and may help diagnose diseases associated with second-harmonic generating tissues such as collagens, muscles, and lipids. Our methodology is especially useful in microendoscopy applications where polarization-controlling optical components can not be easily positioned between the dichroic mirror and the focusing objective.

2 Mathematical Analysis

The design of our ellipticity compensation scheme is shown in Fig. 1. Consider an optical component with a phase retardation δ for light polarized along the x axis with respect to light polarized along the y axis. Moreover, the electric field transmission (or reflection) coefficients along the x and y axes are η_x and η_y , respectively (the transmission or reflection ratio parameter γ is defined to be $\gamma = \eta_x / \eta_y$). The angles of the optical axes of all optical components are measured relative to the x axis. As a result, the transmission or reflection of linearly polarized light by such an optical component would result in elliptically polarized light. To obtain linearly polarized light with the desired output polarization angle θ on reflecting from or transmitting through such an optical component, one can deliver onto the optical component a corresponding elliptically polarized light with particular ellipticity and polarization direction β to offset the polarization ellipticity altering effect of the optical component.

As shown in Fig. 1, ellipticity compensation can be achieved by the use of a half-wave plate (HWP) and a quarter-wave plate (QWP) at the respective angles of $\alpha/2$ and β (Senarmont compensator).¹⁹ Although the ellipticity altering effect of an optical component can be corrected for using a linear polarizer and a QWP, the rotation of a linear polarizer can result in excitation beam translation and contribute to variations in scan field nonuniformity. Therefore, we used a HWP and linearly polarized light as input instead of the combination of a linear polarizer and circularly polarized light to achieve ellipticity compensation. Mathematically, our approach involves the derivation of a relationship between the angles α , β , and θ and the physical parameters δ and γ . We show that for a given set of δ and γ , unique angular combinations of α and β can be used to obtain the desired output polarization angle θ .

When a linearly polarized light along the x axis with angular frequency ω passes through a HWP oriented at an angle $\alpha/2$ relative to the x axis, the electric field can be written as

$$\mathbf{E} = E_0 \cos \alpha \sin \omega t \hat{\mathbf{x}} + E_0 \sin \alpha \sin \omega t \hat{\mathbf{y}}, \quad (1)$$

where E_0 is the amplitude of the electric field. If β is the angle of the slow axis of the QWP relative to the x axis, the excitation electric field, after passing through the QWP, becomes

$$\mathbf{E} = E_0(\cos \beta \cos \varphi \sin \omega t - \sin \beta \sin \varphi \cos \omega t) \hat{\mathbf{x}} + E_0(\sin \beta \cos \varphi \sin \omega t + \cos \beta \sin \varphi \cos \omega t) \hat{\mathbf{y}}, \quad (2)$$

where $\varphi = \alpha - \beta$ is the angle between the excitation polarization after the HWP and the slow axis of the QWP. After reflecting from or passing through an optical component that introduces a phase retardation δ and a transmission or reflection ratio parameter γ , the electric field then becomes

$$\mathbf{E} = E_0(\cos \beta \cos \varphi \sin \omega t - \sin \beta \sin \varphi \cos \omega t) \hat{\mathbf{x}} + \gamma E_0[\sin \beta \cos \varphi \sin(\omega t + \delta) + \cos \beta \sin \varphi \cos(\omega t + \delta)] \hat{\mathbf{y}}. \quad (3)$$

By expanding $\sin(\omega t + \delta)$ and $\cos(\omega t + \delta)$ and rearranging the time-independent components, the resulting electric field can be expressed as

$$\mathbf{E} = E_0(d_1 \sin \omega t + d_2 \cos \omega t) \hat{\mathbf{x}} + E_0(d_3 \sin \omega t + d_4 \cos \omega t) \hat{\mathbf{y}}, \quad (4)$$

where $d_1 = \cos \beta \cos \varphi$, $d_2 = -\sin \beta \sin \varphi$, $d_3 = \gamma(\sin \beta \cos \varphi \cos \delta - \cos \beta \sin \varphi \sin \delta)$, and $d_4 = \gamma(\sin \beta \cos \varphi \sin \delta + \cos \beta \sin \varphi \cos \delta)$ are all time-independent factors. To generate a linearly polarized output, the ratio between the x and y components of the electric field must remain constant at all time. This is a condition satisfied when $d_3/d_1 = d_4/d_2$. Substituting the expressions for d_1 , d_2 , d_3 , and d_4 into the preceding relation, a quadratic relation in $\tan \varphi$, with the two roots can be obtained

$$\tan \varphi_{\pm} = \frac{1 \pm (1 + \sin^2 2\beta \tan^2 \delta)^{1/2}}{\sin 2\beta \tan \delta}. \quad (5)$$

The absence of γ in Eq. (5) shows that the ratio of the transmission or reflection ratio parameter has no effect on the linearity of incident polarization. Only the phase retardation δ can influence the ellipticity of the output polarization. Since the product of the two solutions $(\tan \varphi_+)(\tan \varphi_-) = -1$, the two unique angles φ_+ and φ_- differ by 90 deg. For an optical component with a phase retardation δ , for every QWP orientation, there are two corresponding α angles, within 180 deg, that will result in a linearly polarized output. Figure 2(a) shows the generalized solution of relative polarization angle φ for various combinations of the QWP angle β and the phase retardation angle δ .

To determine the QWP angle β , we substitute the solution for φ into the relation $\tan \theta = E_y/E_x$, and obtain the output polarization equation as a function of γ , β , and δ .

$$\tan \theta = \gamma \tan \beta \cos \delta - \gamma \tan \varphi \sin \delta. \quad (6)$$

Solving Eq. (6) for β and substituting Eq. (5) for $\tan \varphi$, we can obtain the QWP angle as a function of the optical component's retardation δ , the transmission or reflection ratio pa-

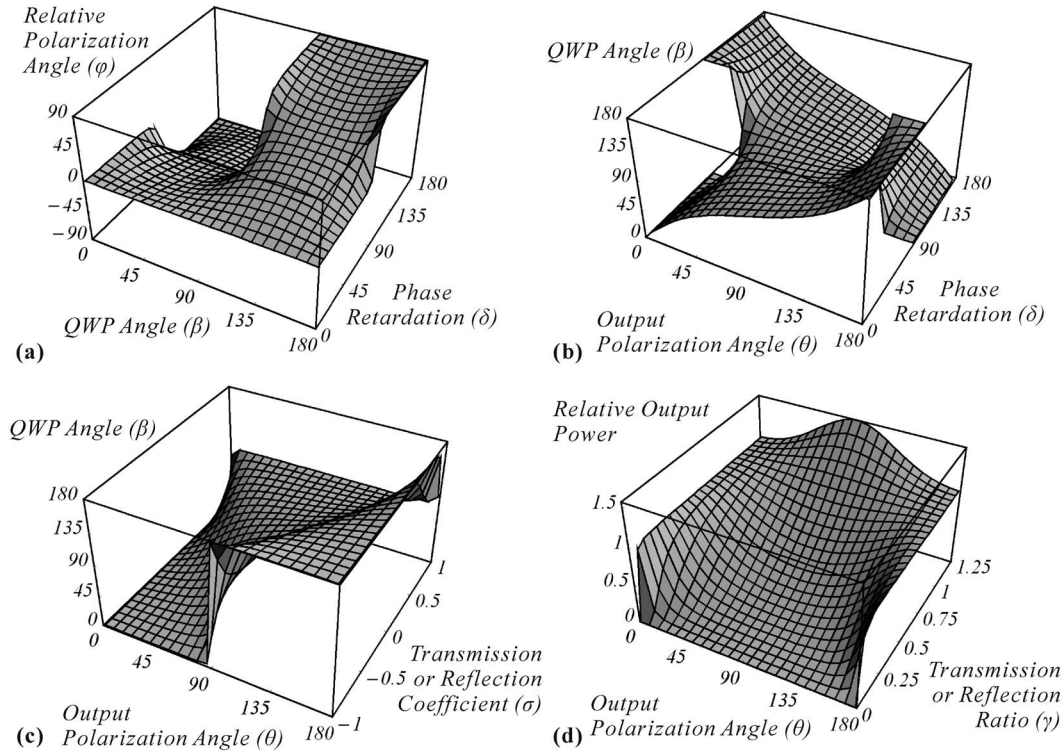


Fig. 2 Calculated results of the relationship between (a) relative polarization angle, QWP angle, and phase retardation; (b) output polarization angle, QWP angle, and phase retardation when the transmission or reflection ratio γ is 0.6; (c) output polarization angle, QWP angle, and transmission or reflection ratio when the phase retardation δ is 45 deg; and (d) relative output power, output polarization angle, and transmission or reflection ratio.

parameter γ , and the orientation of the output polarization angle θ :

$$\tan \beta_{\pm} = \frac{\gamma^2 - \tan^2 \theta \pm (\gamma^4 + \tan^4 \theta + 2\gamma^2 \cos 2\delta \tan^2 \theta)^{1/2}}{-2\gamma \cos \delta \tan \theta} \quad (7)$$

Equation (7) shows that for an optical component with particular values of retardation angle and transmission or reflection ratio parameter, it is possible to obtain all possible output polarization angle θ by varying the QWP angle. To demonstrate our results, we fixed the ratio of transmission efficiency at $\gamma=0.6$ and allow the retardation angle to vary [Fig. 2(b)]. In Fig. 2(c), we fixed the retardation angle $\delta=45$ deg and allow the ratio of transmission or reflection efficiency to vary. Note that we defined $\sigma = [(1-\gamma)/(1+\gamma)] = [(\eta_x - \eta_y)/(\eta_x + \eta_y)]$ such that σ , the ratio of the relative difference of the transmission or reflection ratio between the x and y axes, varies from -1 to $+1$ for all values of γ . It follows from the definition that σ varies from $+1$ to -1 as γ increases from zero to infinity. In this case, we found that $(\tan \beta_+) (\tan \beta_-) = -1$, indicating that the two QWP solutions differ by 90 deg.

In practice, with known values of the two parameters δ and γ , we can use Eq. (7) to obtain the needed QWP angle for the desired output polarization angle. For example, to obtain an output polarization angle of 60 deg, the QWP needs to be 45 deg. From there, the QWP angle can be used in Eq. (5) to obtain the corresponding relative polarization angle, which is 158 deg in this case.

Since γ is variable, the relative output power will be different for different output polarization orientations. Note that the input power of linearly polarized light, P_i (proportional to E^2) remains unchanged as light passed through HWP and QWP. To obtain a relation between the output polarization orientation and power, we must know the actual transmission or reflection efficiencies rather than their ratio. After transmitting through or reflecting from the optical component, the electric field obeys the relation $\tan^2 \theta = E_y^2/E_x^2$. As a result, the output power can be expressed as

$$P_0 = \frac{E_x^2 + E_y^2}{[(E_x/\eta_x)^2 + (E_y/\eta_y)^2]} P_i \quad (8)$$

Therefore, the expression for the relative output power becomes

$$P_0 = \eta_x^2 \gamma^2 \left(\frac{1 + \tan^2 \theta}{\gamma^2 + \tan^2 \theta} \right) P_i \quad (9)$$

After normalization by the factor $\eta_x^2 P_i$, the relative output power as a function of the output polarization angle θ and the ratio of transmission or reflection ratio parameter γ is plotted in Fig. 2(d). Note that η_x is an overall multiplicative parameter, which does not affect the relative power but only affect the range of γ . In the example plotted in Fig. 2(d), we arbitrarily choose $\eta_x=0.8$ and vary γ from 0 to 1.25. In actual experiments, the specific γ value must be determined to obtain the dependence of output angles on relative output power.

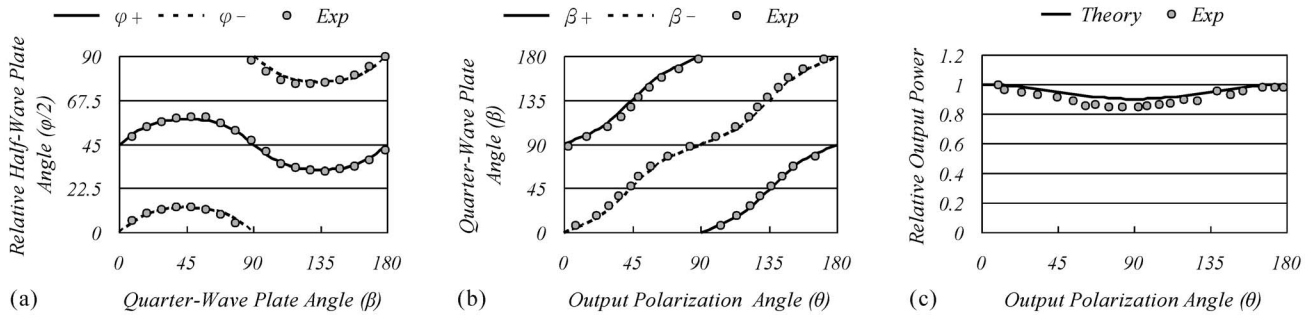


Fig. 3 Data points and mathematical calculation: (a) the combinations of relative HWP and QWP angles that output linearly polarized light, (b) relationship between the QWP and output linear polarization angles, and (c) relative output power as a function of output polarization angle.

The calibration curve can then be used to correct for the effect due to power variations from varying the output polarization angles.

3 Equipment, Material, and Method

The homebuilt epi-illuminated laser scanning SHG microscope used in this study is similar to one that has been previously described.²⁰ The excitation source is a pulsed ti:sapphire laser (Tsunami, Spectral Physics, Mountain View, California) tuned to 780 nm. The main dichroic filter used in the system is a short-pass dichroic mirror (700dcspxruv-2p, Chroma Technology, Rockingham, Vermont), and a narrow-band pass filter (HQ390-22m-2p, Chroma Technology) is used to select the SHG signal (390 ± 10 nm). We used a Fluor, 40 \times /NA 0.8 water immersion objective (Nikon, Japan). The use of an NA 0.8 objective is motivated by the fact that a previous study showed that objectives with higher NA values than 0.8 can alter the polarization of the excitation light.²¹ The lateral resolution of our SHG system is estimated to be²² 0.42 μm .

Experimentally, a linear polarizer and a power meter were used to verify the output polarization state. In our approach, for every 10-deg change in the QWP angle, we rotated the HWP and the linear polarizer in front of the power meter to determine the angular combination that results in linearly polarized output. The angular range of the QWP is 0 to 180 deg and that of the HWP is 0 to 90 deg. Since the HWP requires only 90 deg to rotate the polarization of linearly polarized light within the 180 deg range, the equation of HWP angle $\alpha/2$ is $\alpha/2 = (\phi + \beta)/2$. The angular positions of the QWP, the HWP, and the linear polarizer were recorded after satisfying the condition of at least an 100:1 rejection of the cross-polarization intensities as the linear polarizer was rotated.

The rat tail tendon sample used in our experiment came from an 8-week-old rat. After the rat was sacrificed, its tail was cut and stored at -80°C until right before experimentation. As in previous studies, we found that the process of freezing and thawing do not affect SHG imaging (our unpublished data and Ref. 23). At room temperature, a small piece of rat tail tendon around 2 cm in length was cut and immersed in phosphate-buffered saline solution. The wet tendon was then placed on a glass slide and sealed with a cover glass. The mouse leg muscle specimen came from a 6-week-old mouse after sacrifice and preparation was similar as for rat tail tendon.

We used a theoretical model with variable parameters to investigate the excitation polarization SHG properties of fibril of cylindrical symmetry.²³ In analyzing the polarization resolved SHG images, we adopted the following second order polarization model

$$\mathbf{P} = a\mathbf{s}(\mathbf{s} \cdot \mathbf{E})^2 + b\mathbf{s}(\mathbf{E} \cdot \mathbf{E}) + c\mathbf{E}(\mathbf{s} \cdot \mathbf{E}). \quad (10)$$

In Eq. (10), \mathbf{s} is the unit vector lying along the collagen fiber axis and \mathbf{E} is the incident electric field; a , b , and c are coefficients relating to the second-order susceptibility tensor, and the least-squares method can be used to fit to study their properties. In this model, the emitted SHG signal intensity is sensitive to the linear polarization angle of excitation light.¹⁴ The dependence of SHG intensity on the incident polarization can be described as

$$I \propto E_0^4 [(d_{31} \sin^2 \phi + d_{33} \cos^2 \phi)^2 + (d_{15} \sin 2\phi)^2], \quad (11)$$

where d_{31} , d_{33} , and d_{15} are the contracted notation of the susceptibility tensor, where $d_{31}=b$, $d_{15}=c/2$, $d_{33}=a+b+c$, and ϕ is the angle between the polarization direction of linearly polarized excitation and the long axis of the fibril.^{14,24} To verify the validity of our approach, the ellipticity compensation method was applied to see if the sample-rotating data fits our results well. Least-squares fitting was performed with the IDL program (ITT Visual Information Solutions). We selected 21 evenly spaced linear polarization output angles and used them to obtain excitation polarization-resolved SHG images of rat tail tendon and mouse leg muscle. The $55 \times 55 \mu\text{m}$ image area was scanned at 256×256 pixels resolution. To minimize sample birefringence effects, the SHG images were acquired at approximately $5 \mu\text{m}$ below the specimen surface. For each angle, we scanned the specimens three times and averaged the images in forming a final set of images for second-order susceptibility analysis. Graphically, the SHG intensity variation within the analyzed regions is indicated by error bars.

4 Results and Discussion

One task we performed was to verify the relationship between the QWP angles, HWP angles, output polarization angles, and relative output power. Figures 3(a)–3(c) show the experimental results (dots) and the theoretical prediction (curved lines) of our results. The curves were obtained from the mathematical calculation using the independently obtained phase retar-

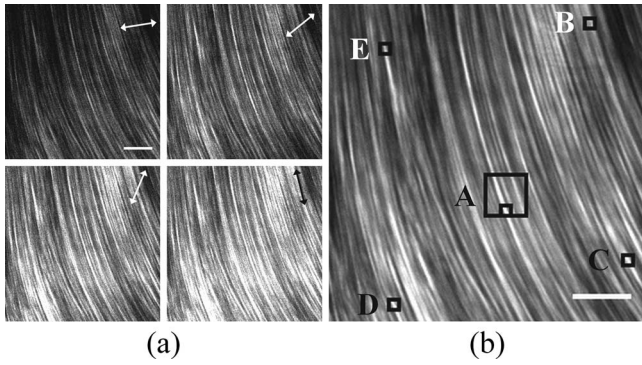


Fig. 4 Excitation polarization resolved SHG images of rat tail tendon fibrils: (a) SHG images at different angles of excitation polarization and (b) average of SHG images acquired at 21 polarization angles. Block boxes represent the different area analyzed for SHG dependence on excitation polarization angles. Scale bar =10 μm.

dation angle and the x and y reflection coefficients of the main dichroic mirror. For the dichroic mirror used in our study, the phase retardation was determined to be -52 deg and the ratio of reflection coefficients (x to y axes) of the electric field was determined to be 0.97. These values were obtained using different angles of linearly polarized light incident onto the dichroic mirror and measuring the ellipticity of reflected excitation source. Figure 3(a) shows the combinations of relative HWP and QWP angles that achieve linearly polarized output, and the result shown in Fig. 3(b) is the linear polarization angles with the associated QWP angles.

Furthermore, we compared the angular dependence of fluorescence intensity with the theoretical prediction, by using an aqueous fluorescein sample. Due to the two-photon fluorescence excitation process, the fluorescence intensity F , which depends quadratically on the excitation intensity, is given by

$$F \propto \gamma^4 \left(\frac{1 + \tan^2 \theta}{\gamma^2 + \tan^2 \theta} \right)^2. \quad (12)$$

In Eq. (12), θ represents the linear polarization output angle, and γ represents the ratio of reflection coefficients of the x axis relative to that of the y axis. The comparison of the mathematical result with experimental data is shown in Fig. 3(c). While there is general agreement between the theoretical calculation and the experimental results, a small shift (6% maximum) does exist.

To validate our approach, we scanned the rat tail tendon and the mouse leg muscle, which is mainly composed of type I collagen fibers and myofibrils. Figure 4(a) presents the SHG images of tendon fibrils scanned using the excitation of four

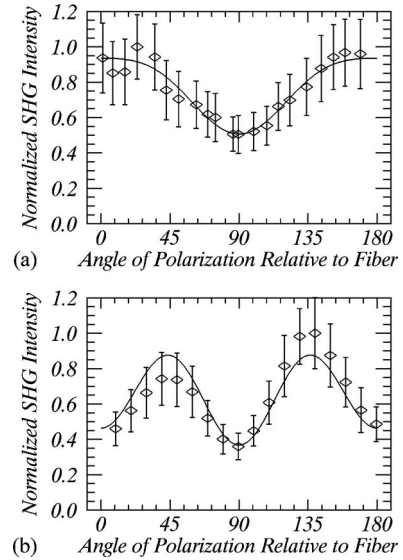


Fig. 5 Model fitting of SHG intensity variation with excitation polarization angles (a) with ellipticity compensation of wave plates and (b) without ellipticity compensation and rotating the HWP only. (Diamonds: experimental data; solid lines: fitted curves.)

different linear polarization angles, as indicated by the arrow directions. From the figure, it is clear that the SHG signal varies significantly with the different excitation polarization angles. The SHG intensity tends to be higher when the direction of the linear polarization is paralleled to the fiber and decreases as the polarization direction becomes perpendicular to the fibers. In using Eq. (11) to analyze the excitation polarization-resolved SHG images, we obtained results similar to the graph shown in Fig. 5(a). The data in Fig. 5 correspond to the average intensity of a 5×5 -pixel square shown by the small black box A in the center of Fig. 4(b), and error bars are the standard deviations of intensity within 25 pixels in area. Previous result assumed that $c=2b$ in Eq. (11) and $r=b/a$, which is the only variable of normalized SHG intensity.²³ Our model fitting leads to the susceptibility tensor element ratio of $r=-0.70 \pm 0.05$, consistent with $r=-0.71 \pm 0.05$ obtained by sample rotation (our unpublished data) and -0.73 obtained by Stoller et al.²³ Note in Fig. 5 that the angles shown on the x axis are measured counterclockwise with respect to the orientation of the fiber, which at our selected square is 13 deg counterclockwise relative to the vertical direction of the image. Figure 5(b) is the fitting of the SHG signal in the same area without wave plates compensation, where the polarization is assumed to be unaffected by the dichroic mirror and is rotated by HWP. In our experiment, the intensity variation is asymmetric and model fitting gives

Table 1 The γ fitting results at different areas within the SHG image.

	A (small area)	B	C	D	E	A (large area)
With compensation	-0.70 ± 0.05	-0.73 ± 0.03	-0.69 ± 0.03	-0.72 ± 0.04	-0.74 ± 0.05	-0.72 ± 0.04
Without compensation	-0.52 ± 0.02	-0.52 ± 0.01	-0.53 ± 0.02	-0.53 ± 0.02	-0.51 ± 0.02	-0.53 ± 0.02

The boxed regions of A, B, C, D, and E are the areas in Fig. 4(b) selected for excitation polarization SHG analysis.

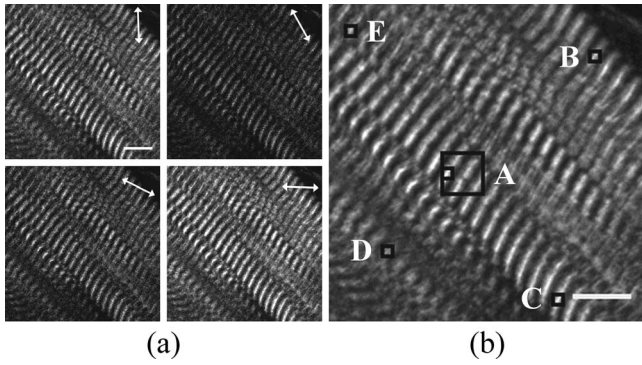


Fig. 6 Excitation polarization resolved SHG images of mouse leg muscle myofibrils: (a) dependence of SHG intensity on excitation polarization angles (arrows indicate excitation polarization orientations) and (b) average of SHG images at 21 different excitation polarization angles. The boxed regions represent the different areas analyzed for excitation polarization dependence. Scale bar = 10 μm .

$r = -0.52 \pm 0.02$, which deviates significantly from previous results. To further test our polarization ellipticity compensation method, we also performed analysis at both large area (30 \times 30 pixels) and four corners, whose positions are shown by black boxes in Fig. 4(b), and the results are shown by Table 1.

It is clear that, with our polarization ellipticity compensation scheme, the fitting result of γ agrees well at different locations within the SHG image. One advantage of our compensation method is that we can analyze a relatively small area when rotating the polarization of light at the scale of a single fibril.

In addition, we scanned and tested our methodology in the SHG imaging of the mouse leg, which is another fibrous tissue capable of producing intense SHG signal. Figure 6(a) shows the SHG intensity change at different excitation polarization angles. As performed with the rat tail tendon sample, we performed the parameter fitting in Eq. (11) on the muscle sample, and the result is shown in Fig. 7. The muscle SHG comes from myofibril, and it was shown⁸ that the fitting parameters can be used to derive the pitch angle θ of myosin rod by the relation $\tan^2 \theta = 2d_{31}/d_{33}$. In this manner, the myosin rod pitch angle was determined to be 61.2 deg, as measured by Plotnikov et al.⁸

Our analysis result is shown in Table 2. In all regions analyzed, the derived values of the pitch angle are closer to previous published results when the ellipticity scheme was applied.

Based on these results, we conclude that our approach can be used to achieve polarization-resolved SHG imaging without specimen rotation and that the polarization ellipticity al-

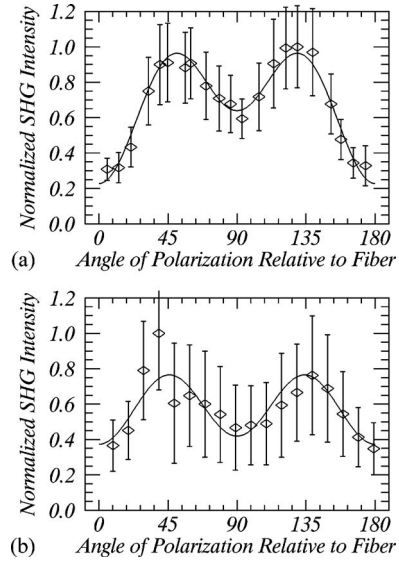


Fig. 7 Model fitting of SHG intensity variation with excitation polarization angles: (a) with polarization compensation of wave plates, where the analyzing area of 5 \times 5 pixels is shown by the boxed region in the center of Fig. 6, and (b) without compensation and rotating HWP only. (Diamonds: experimental data; solid lines: fitted curves.)

tering properties of optical components such as the dichroics can be corrected for. This work shows that our method of using polarization rotation of excitation light enables us to more easily analyze data and with more precision.

5 Conclusion

We performed the necessary mathematical analysis and devised an experimental approach for compensating the ellipticity altering effect of an optical component using a QWP and a HWP. We demonstrated that linearly polarized output with the controlled polarization angle perpendicular to the direction of propagation can be achieved for excitation-polarization-resolved SHG microscopy. For an optical component with known phase retardation δ and ratio of *s*- and *p*- waves transmission or reflection coefficient γ , we can determine the angular positions of the added wave plates to achieve output with arbitrary linear polarization angles. The rotation of wave plates can be automated using motorized rotary stages controlled by computer. One can envision the combination of our methodology and a fast-scanning, video-rate SHG microscope that can greatly reduce the data acquisition in achieving specimen-fixed, excitation-polarization-resolved SHG microscopy. Experimentally, our approach was used to achieve excitation-polarization-resolved SHG imaging of type I collagen fibers in a rat tail tendon and myofibrils in a mouse leg

Table 2 Fitted pitch angles at different areas within the SHG image.

	A (small area)	B	C	D	E	A (large area)
With compensation (deg)	61.7 \pm 1.3	61.4 \pm 1.3	61.5 \pm 1.5	61.0 \pm 1.3	60.9 \pm 1.7	60.6 \pm 1.4
Without compensation (deg)	55.4 \pm 2.1	55.3 \pm 1.9	55.6 \pm 1.7	56.1 \pm 2.0	55.4 \pm 2.1	56.6 \pm 1.6

A, B, C, D, and E are the boxed regions in Fig. 6(b) selected for the excitation polarization SHG analysis.

muscle, and the results demonstrate that polarized SHG microscopy can be achieved without specimen rotation. Our method is applicable for delivering the desired polarization of excitation light in cases where there are optical components that contribute to ellipticity-altering effects by properly controlling the relative angular orientations between a HWP and a QWP. Our methodology is invaluable for excitation-polarization-resolved SHG experiments in a number of ways. First, image processing and the potential artifacts associated with the sample rotation approach are eliminated. Furthermore, our approach can be conveniently applied to microendoscopy applications where polarization-compensating components can not be easily positioned between the dichroic mirror and the focusing objective. Finally, in principle, our methodology is generally applicable to correcting the ellipticity-altering artifacts in deep-tissue, excitation-polarization-resolved SHG microscopy provided that the specimen birefringence properties are known. This technique has potential biological and medical applications, such as monitoring molecule changes in tissues and organs with a strong SHG signal and fluorescence polarization measurement in providing orientation information of fluorescent molecules in systems such as cell membranes.

Acknowledgments

We acknowledge the support of the National Research Program for Genomic Medicine (NRPGM) and the National Science Council of Taiwan (NSC-95-3112-B-002-018). This work was completed using the Optical Molecular Imaging Microscopy Core Facility (A5) of NRPGM.

References

1. J. B. Pawley, *Handbook of Biological Confocal Microscopy*, Springer, (2006).
2. P. T. C. So, C. Y. Dong, B. R. Masters, and K. M. Berland, "Two-photon excitation fluorescence microscopy," *Annu. Rev. Biomed. Eng.* **2**, 399–429 (2000).
3. R. Oldenbourg, "A new view on polarization microscopy," *Nature* **381**(6585), 811–812 (1996).
4. C. E. Bigelow, D. L. Conover, and T. H. Foster, "Confocal fluorescence spectroscopy and anisotropy imaging system," *Opt. Lett.* **28**(9), 695–697 (2003).
5. Y. Sun, W. Lo, S. J. Lin, S. H. Jee, and C. Y. Dong, "Multiphoton polarization and generalized polarization microscopy reveal oleic-acid-induced structural changes in intercellular lipid layers of the skin," *Opt. Lett.* **29**(17), 2013–2015 (2004).
6. P. J. Campagnola and L. M. Loew, "Second-harmonic imaging microscopy for visualizing biomolecular arrays in cells, tissues and organisms," *Nat. Biotechnol.* **21**(11), 1356–1360 (2003).
7. W. R. Zipfel, R. M. Williams, R. Christie, A. Y. Nikitin, B. T. Hyman, and W. W. Webb, "Live tissue intrinsic emission microscopy using multiphoton-excited native fluorescence and second harmonic generation," *Proc. Natl. Acad. Sci. U.S.A.* **100**(12), 7075–7080 (2003).
8. S. V. Plotnikov, A. C. Millard, P. J. Campagnola, and W. A. Mohler, "Characterization of the myosin-based source for second-harmonic generation from muscle sarcomeres," *Biophys. J.* **90**(2), 693–703 (2006).
9. S. W. Teng et al., "Multiphoton autofluorescence and second-harmonic generation imaging of the ex vivo porcine eye," *Invest. Ophthalmol. Visual Sci.* **47**(3), 1216–1224 (2006).
10. A. Zoumi, A. Yeh, and B. J. Tromberg, "Imaging cells and extracellular matrix in vivo by using second-harmonic generation and two-photon excited fluorescence," *Proc. Nat. Acad. Sci. U.S.A.* **99**(17), 11014–11019 (2002).
11. E. B. Brown, R. B. Campbell, Y. Tsuzuki, L. Xu, P. Carmeliet, D. Fukumura, and R. K. Jain, "In vivo measurement of gene expression, angiogenesis and physiological function in tumors using multiphoton laser scanning microscopy," *Nat. Med.* **7**(7), 864–868 (2001).
12. H. Y. Tan et al., "Multiphoton fluorescence and second harmonic generation imaging of the structural alterations in keratoconus ex vivo," *Invest. Ophthalmol. Visual Sci.* **47**(12), 5251–5259 (2006).
13. M. G. Lin et al., "Evaluation of dermal thermal damage by multiphoton autofluorescence and second-harmonic-generation microscopy," *J. Biomed. Opt.* **11**(6), 064006 (2006).
14. S. W. Chu, S. Y. Chen, G. W. Chern, T. H. Tsai, Y. C. Chen, B. L. Lin, and C. K. Sun, "Studies of $x(2)/x(3)$ tensors in submicron-scaled bio-tissues by polarization harmonics optical microscopy," *Biophys. J.* **86**(6), 3914–3922 (2004).
15. P. Carmeliet and R. K. Jain, "Angiogenesis in cancer and other diseases," *Nature* **407**(6801), 249–257 (2000).
16. F. C. Li, C. C. Wang, S. J. Lin, S. H. Jee, W. Lo, and C. Y. Dong, "Dorsal skin fold chamber for high resolution multiphoton imaging," *Opt. Quantum Electron.* **37**(13–15), 1439–1445 (2005).
17. A. M. Pena, T. Boulesteix, T. Dartigalongue, and M. C. Schanne-Klein, "Chiroptical effects in the second harmonic signal of collagens I and IV," *J. Am. Chem. Soc.* **127**(29), 10314–10322 (2005).
18. D. Debarre, W. Supatto, A. M. Pena, A. Fabre, T. Tordjmann, L. Combettes, M. C. Schanne-Klein, and E. Beaufrepaire, "Imaging lipid bodies in cells and tissues using third-harmonic generation microscopy," *Nat. Methods* **3**(1), 47–53 (2006).
19. P. Hariharan, "The Senarmont compensator—an early application of the geometric phase," *J. Mod. Opt.* **40**(11), 2061–2064 (1993).
20. Y. Sun, J. W. Su, W. Lo, S. J. Lin, S. H. Jee, and C. Y. Dong, "Multiphoton polarization imaging of the stratum corneum and the dermis in ex-vivo human skin," *Opt. Express* **11**(25), 3377–3384 (2003).
21. B. Richards and E. Wolf, "Electromagnetic diffraction in optical systems. 2. Structure of the image field in an aplanatic system," *Proc. R. Soc. London Ser. a Math. Phys. Sci.* **253**(1274), 358–379 (1959).
22. R. Gauderon, P. B. Lukins, and C. J. R. Sheppard, "Three-dimensional second-harmonic generation imaging with femtosecond laser pulses," *Opt. Lett.* **23**(15), 1209–1211 (1998).
23. P. Stoller, B. M. Kim, A. M. Rubenchik, K. M. Reiser, and L. B. Da Silva, "Polarization-dependent optical second-harmonic imaging of a rat-tail tendon," *J. Biomed. Opt.* **7**(2), 205–214 (2002).
24. R. W. Boyd, *Nonlinear Optics*, Academic Press, (2003).